https://doi.org/10.15407/ujpe66.10.908

A.V. KOROTUN,[1] YA.V. KARANDAS,[1] V.I. REVA,[1] I.M. TITOV [2]

[1] Zaporizhzhya National Technical University
(64, Zhukovs'kogo Str., Zaporizhzhya 69063, Ukraine; e-mail: andko@zntu.edu.ua)
[2] UAD Systems
(84, Oleksandrivs'ka Str., Zaporizhzhya (69002, Ukraine))

POLARIZABILITY OF TWO-LAYER METAL-OXIDE NANOWIRES

Frequency dependences have been obtained for the real and imaginary parts and the absolute values of the components of the polarizability tensor of metal-oxide nanowires, as well as for the absorption and scattering cross-sections. The limiting cases of the 'thick " and "thin " outer oxide layers are studied. Numerical calculations are performed for Al, Cu, and Ag wires coated with a corresponding oxide layer. The models where the dielectric constant of an oxide is either a constant or a function of the frequency are considered. In the last case, experimental frequency dependences of the refractive and extinction indices are used. The influence of the oxide layer thickness on the frequency dependences of the polarizability and the absorption and scattering cross-sections is analyzed. It is found that the presence of an oxide leads to a decrease in the frequency of surface plasmons in two-layer nanowires due to the influence of classical size effects.

K e y w o r d s: metal-oxide nanowire, polarization tensor, absorption cross-section, scattering cross-section, surface plasmons, dielectric function, size effect.

1. Introduction

Metal nanowires are widely used in modern nanotechnology as elements of interconnections in nanoelectronic circuits, optical communication channels, and building blocks in sensors [1–8]. Such a variety of potential applications is based on the phenomenon of surface plasmon resonance. The spectral position of the latter is determined by the size and shape of the nanowire cross-section, as well as the optical properties of the nanowire metal and the environment [3, 9–15].

Resonance phenomena occurring at the interaction of electromagnetic radiation with nanostructures are powerful energy and information factors for the creation of novel nanophotonic technologies [16]. The plasmon resonance effect, which takes place in metal nanoparticles and nanostructures of various shapes and nature, opens opportunities for the controlled scattering of light belonging to a certain spectral interval in a given direction. It also allows the electromagnetic field to be localized at the nanoscale [17]. In addition, the application of resonance micro- and nanostructures can significantly improve the characteristics of the components in photovoltaic, photocatalytic, biophotonic, and other systems [18–23].

Owing to the natural oxidation of a metal on the surface of nanostructures in a liquid or gaseous environment [24, 25], the formation of an oxide layer is possible. In particular, when studying the optical properties of spherical metal nanoparticles [26], the account for the presence of an oxide layer on the nanoparticle surface brings about good agreement between the results of theoretical calculations and experimental measurements. It is reasonable to expect the same in the case of systems with other geometries,

in particular, metal nanowires. Therefore, the study of the optical properties of metal-oxide nanowires is challenging.

Hence, the aim of this work is to study the frequency dependences of the polarizability and the absorption and scattering cross-sections of a metal nanocylinder coated with an oxide layer and placed in a dielectric medium, as well as the particle-size dependence of the surface plasmon resonance frequency.

2. Formulation of the Problem and Basic Relations

2.1. General relations

Consider a two-layer metal-oxide nanowire with an oxide layer of the thickness $t = b - a$, where a is the radius of the metal core, and b is the total radius of the nanowire, The nanowire is in a medium with the dielectric constant $\epsilon_{\rm m}$ (see Fig. 1). Due to the anisotropy and a mismatch between the directions of the dipole moment, $\mathbf{p}$, and external electric field strength, $\mathscr{E}_0$, vectors, the polarizability of the system is a diagonal tensor of the second rank

$$\alpha_{@} = \begin{pmatrix} \alpha_{@}^{\perp} & 0 & 0 \\ 0 & \alpha_{@}^{\perp} & 0 \\ 0 & 0 & \alpha_{@}^{\parallel} \end{pmatrix}, \tag{1}$$

where the expressions for the components $\alpha_{@}^{\perp(\parallel)}$ are obtained from the relations for a two-layer elongated ellipsoid of revolution [27],

$$\alpha_{@}^{\perp(\parallel)} = V \frac{\Lambda_{\perp(\parallel)}}{{\rm Z}_{\perp(\parallel)}}. \tag{2}$$

Here,

$$\Lambda_{\perp(\parallel)} = \left(\epsilon_{\rm s}^{\perp(\parallel)} - \epsilon_{\rm m}\right)\left[\epsilon_{\rm s}^{\perp(\parallel)} + \left(\epsilon_{\rm c}^{\perp(\parallel)} - \epsilon_{\rm s}^{\perp(\parallel)}\right) \times \right.$$
$$\left. \times \left(\mathcal{L}_{\perp(\parallel)}^{(1)} - \beta_{\rm c}\mathcal{L}_{\perp(\parallel)}^{(2)}\right)\right] + \beta_{\rm c}\epsilon_{\rm s}^{\perp(\parallel)}\left(\epsilon_{\rm c}^{\perp(\parallel)} - \epsilon_{\rm s}^{\perp(\parallel)}\right), \tag{3}$$

$${\rm Z}_{\perp(\parallel)} = \left[\epsilon_{\rm s}^{\perp(\parallel)} + \left(\epsilon_{\rm c} - \epsilon_{\rm s}^{\perp(\parallel)}\right)\left(\mathcal{L}_{\perp(\parallel)}^{(1)} - \beta_{\rm c}\mathcal{L}_{\perp(\parallel)}^{(2)}\right)\right] \times$$
$$\times \left[\epsilon_{\rm m} + \left(\epsilon_{\rm s}^{\perp(\parallel)} - \epsilon_{\rm m}\right)\mathcal{L}_{\perp(\parallel)}^{(2)}\right] +$$
$$+ \beta_{\rm c}\mathcal{L}_{\perp(\parallel)}^{(2)}\epsilon_{\rm s}^{\perp(\parallel)}\left(\epsilon_{\rm c} - \epsilon_{\rm s}^{\perp(\parallel)}\right), \tag{4}$$

and $\epsilon_{\rm c}^{\perp(\parallel)}$ and $\epsilon_{\rm s}^{\perp(\parallel)}$ are the transverse ($\perp$) and longitudinal ($\parallel$) components of the dielectric constants of the core and shell materials, respectively; $\mathcal{L}_{\perp(\parallel)}^{(1)}$ and $\mathcal{L}_{\perp(\parallel)}^{(2)}$ are the transverse and longitudinal depolarization coefficients of the inner and outer layers, respectively; $\beta_{\rm c} = V_c/V$; V_c is the inner ellipsoid volume; and V the total ellipsoid volume.

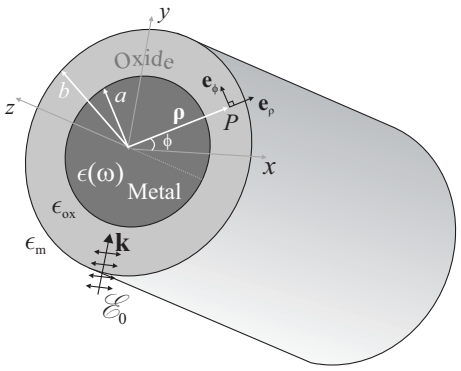

Fig. 1. Geometry of the problem

Expression (2) can be written in a more compact form similar to the expression for the polarizability of a metal ellipsoid of revolution,

$$\alpha_{@}^{\perp(\parallel)} = V \frac{\epsilon_{@}^{\perp(\parallel)} - \epsilon_{\rm m}}{\epsilon_{\rm m} + \mathcal{L}_{\perp(\parallel)}^{(2)}\left(\epsilon_{@}^{\perp(\parallel)} - \epsilon_{\rm m}\right)}, \tag{5}$$

if we introduce the "equivalent" dielectric constant of a two-layer ellipsoid, which is defined by the expression

$$\epsilon_{@}^{\perp(\parallel)} = \epsilon_{\rm s}^{\perp(\parallel)} + \frac{\epsilon_{\rm s}^{\perp(\parallel)}\beta_{\rm c}\left(\epsilon_{\rm c}^{\perp(\parallel)} - \epsilon_{\rm s}^{\perp(\parallel)}\right)}{\epsilon_{\rm s}^{\perp(\parallel)} + \left(\epsilon_{\rm c}^{\perp(\parallel)} - \epsilon_{\rm s}^{\perp(\parallel)}\right)\left(\mathcal{L}_{\perp(\parallel)}^{(1)} - \beta_{\rm c}\mathcal{L}_{\perp(\parallel)}^{(2)}\right)}. \tag{6}$$

In the case of a two-layer cylinder, $\mathcal{L}_{\perp}^{(1)} = \mathcal{L}_{\perp}^{(2)} = 1/2$, $\mathcal{L}_{\parallel}^{(1)} = \mathcal{L}_{\parallel}^{(2)} = 0$, and $\beta_{\rm c} = (a/b)^2$. So, we obtain

$$\epsilon_{@}^{\perp} = \epsilon_{\rm s}^{\perp}\frac{1 + \beta_{\rm c}\delta_{@}^{\perp}}{1 - \beta_{\rm c}\delta_{@}^{\perp}}, \quad \epsilon_{@}^{\parallel} = \beta_{\rm c}\epsilon_{\rm c}^{\parallel} + (1 - \beta_{\rm c})\,\epsilon_{\rm s}^{\parallel}, \tag{7}$$

where the notation

$$\delta_{@}^{\perp} = \frac{\epsilon_{\rm c}^{\perp} - \epsilon_{\rm s}^{\perp}}{\epsilon_{\rm c}^{\perp} + \epsilon_{\rm s}^{\perp}} \tag{8}$$

was introduced.

Now, let us separately consider two cases: where the dielectric constant of the oxide layer ϵ is a constant, and where it depends on the frequency of incident light.

2.1.1. The case $\epsilon_s^{\perp} = \epsilon_s^{\parallel} = \epsilon_{\rm ox} = {\rm const}$

Using formulas (2)–(8), we may write the following expression for the dimensionless transverse component of the polarizability:

$$\tilde{\alpha}_{@}^{\perp} = \frac{\alpha_{@}^{\perp}}{V} = 2\frac{\epsilon_{\rm c}^{\perp} - \tilde{\epsilon}_{\rm c}^{(-)}}{\epsilon_{\rm c}^{\perp} - \tilde{\epsilon}_{\rm c}^{(+)}} \frac{(1+\beta_{\rm c})\,\epsilon_{\rm ox} - (1-\beta_{\rm c})\,\epsilon_{\rm m}}{(1+\beta_{\rm c})\,\epsilon_{\rm ox} + (1-\beta_{\rm c})\,\epsilon_{\rm m}}, \quad (9)$$

where

$$\tilde{\epsilon}_{\rm c}^{(\pm)} = -\epsilon_{\rm ox}\frac{(1-\beta_{\rm c})\,\epsilon_{\rm ox} \pm (1+\beta_{\rm c})\,\epsilon_{\rm m}}{(1+\beta_{\rm c})\,\epsilon_{\rm ox} \pm (1-\beta_{\rm c})\,\epsilon_{\rm m}}. \quad (10)$$

The equality ${\rm Re}\,\epsilon_{\rm c}^{\perp} = \tilde{\epsilon}_{\rm c}^{(+)}$ is a condition of the surface plasmon resonance, and ${\rm Re}\,\epsilon_{\rm c}^{\perp} = \tilde{\epsilon}_{\rm c}^{(-)}$ is a condition for the numerator in the expression for the polarizability to vanish (the invisibility condition).

Let us consider the limiting cases of "thin" and "thick" oxide layers.

1. Approximation of "thin" oxide layer ($\beta_{\rm c} \to 1$). In this approximation, we have

$$\tilde{\epsilon}_{\rm c}^{(\pm)} = -\epsilon_{\rm ox}\frac{(1-\beta_{\rm c})\,\epsilon_{\rm ox} \pm 2\epsilon_{\rm m}}{2\epsilon_{\rm ox} \pm (1-\beta_{\rm c})\,\epsilon_{\rm m}} =$$

$$= -\epsilon_{\rm m}\left(\frac{1-\beta_{\rm c}}{2}\frac{\epsilon_{\rm ox}}{\epsilon_{\rm m}} \pm 1\right)\left(1 \pm \frac{1-\beta_{\rm c}}{2}\frac{\epsilon_{\rm m}}{\epsilon_{\rm ox}}\right)^{-1} \cong$$

$$\cong -\epsilon_{\rm m}\left(\frac{1-\beta_{\rm c}}{2}\frac{\epsilon_{\rm ox}}{\epsilon_{\rm m}} \pm 1\right)\left(1 \mp \frac{1-\beta_{\rm c}}{2}\frac{\epsilon_{\rm m}}{\epsilon_{\rm ox}}\right) \cong$$

$$\cong -\epsilon_{\rm m}\left[\pm 1 + \frac{1-\beta_{\rm c}}{2}\left(\frac{\epsilon_{\rm ox}}{\epsilon_{\rm m}} - \frac{\epsilon_{\rm m}}{\epsilon_{\rm ox}}\right)\right]. \quad (11)$$

For the dimensionless transverse and longitudinal components of the polarizability, we obtain the formulas

$$\tilde{\alpha}_{@}^{\perp} \simeq \frac{\epsilon_{\rm c}^{\perp} - \tilde{\epsilon}_{\rm c}^{(-)}}{\epsilon_{\rm c}^{\perp} - \tilde{\epsilon}_{\rm c}^{(+)}} \frac{2\epsilon_{\rm ox} - (1-\beta_{\rm c})\,\epsilon_{\rm m}}{2\epsilon_{\rm ox} + (1-\beta_{\rm c})\,\epsilon_{\rm m}} =$$

$$= \frac{\epsilon_{\rm c}^{\perp} - \tilde{\epsilon}_{\rm c}^{(-)}}{\epsilon_{\rm c}^{\perp} - \tilde{\epsilon}_{\rm c}^{(+)}}\left(1 - \frac{1-\beta_{\rm c}}{2}\frac{\epsilon_{\rm m}}{\epsilon_{\rm ox}}\right)\left(1 + \frac{1-\beta_{\rm c}}{2}\frac{\epsilon_{\rm m}}{\epsilon_{\rm ox}}\right)^{-1} \simeq$$

$$\simeq \frac{\epsilon_{\rm c}^{\perp} - \tilde{\epsilon}_{\rm c}^{(-)}}{\epsilon_{\rm c}^{\perp} - \tilde{\epsilon}_{\rm c}^{(+)}}\left(1 - (1-\beta_{\rm c})\,\frac{\epsilon_{\rm m}}{\epsilon_{\rm ox}}\right), \quad (12)$$

$$\tilde{\alpha}_{@}^{\parallel} \simeq \frac{1}{\epsilon_{\rm m}}\left\{\beta_{\rm c}\epsilon_{\rm c}^{\parallel} - \epsilon_{\rm m} + (1-\beta_{\rm c})\,\epsilon_{\rm ox}\right\}. \quad (13)$$

2. Approximation of "thick" oxide layer ($\beta_{\rm c} \to 0$). In this approximation, $\tilde{\epsilon}_{\rm c}^{(+)} = \tilde{\epsilon}_{\rm c}^{(-)} = -\epsilon_{\rm ox}$. So, we have

$$\tilde{\alpha}_{@}^{\perp} = \frac{\epsilon_{\rm ox} - \epsilon_{\rm m}}{\epsilon_{\rm ox} + \epsilon_{\rm m}}, \quad \tilde{\alpha}_{@}^{\parallel} = \frac{\epsilon_{\rm c} - \epsilon_{\rm m}}{\epsilon_{\rm m}}. \quad (14)$$

2.1.2. The case $\epsilon_s^{\perp} = \epsilon_s^{\parallel} = \epsilon_s = \epsilon_{\rm ox}(\omega)$

In the case where the dielectric constant of the oxide is a complex quantity and depends on the frequency, we have $\epsilon_{\rm ox}(\omega) = \epsilon_{\rm ox}^{\rm I}(\omega) + i\epsilon_{\rm ox}^{\rm II}(\omega)$. This is true, e.g., for Ag_2O [28]. To find the frequency dependence of the dielectric function for Ag_2O, we use the corresponding experimental frequency dependences for the refractive, $\bar{n}$, and the excision, $\varkappa$, indices from work [28] (see Fig. 2).

The real and imaginary parts of the dielectric constant of silver oxide are related to $\bar{n}$ and $\varkappa$ via the following formulas:

$$\epsilon_{\rm ox}^{\rm I}(\omega) = \bar{n}^2(\omega) - \varkappa^2(\omega), \quad (15)$$

$$\epsilon_{\rm ox}^{\rm II}(\omega) = 2\bar{n}(\omega)\,\varkappa(\omega). \quad (16)$$

The best approximations to the experimental curves $\bar{n}(\omega)$ and $\varkappa(\omega)$ are the polynomials of the sixth and third orders,

$$\bar{n}(\omega) = \begin{cases} \sum\limits_{i=0}^{6} c_i\omega^i, & \hbar\omega \le 3.3 \text{ eV}; \\ \sum\limits_{i=0}^{3} d_i\omega^i, & \hbar\omega > 3.3 \text{ eV}; \end{cases}$$

$$\varkappa(\omega) = \begin{cases} \sum\limits_{i=0}^{6} \tilde{c}_i\omega^i, & \hbar\omega \le 3.8 \text{ eV}; \\ \sum\limits_{i=0}^{6} \tilde{d}_i\omega^i, & \hbar\omega > 3.8 \text{ eV}; \end{cases}$$

where the coefficients c_i, d_i, $\tilde{c}_i$, and $\tilde{d}_i$ ($i = 0 \ldots 6$) are quoted in Table 1.

In Drude's theory, the dielectric function of a metal nanoconductor is determined by the expression

$$\epsilon(\omega) = \epsilon^{\infty} - \frac{\omega_p^2}{\omega^2 + \gamma^2} + {\rm i}\frac{\omega_p^2\gamma}{(\omega^2+\gamma^2)\,\omega}. \quad (17)$$

Here, $\omega_p = \left(e^2 n_e/\epsilon_0 m^*\right)^{1/2}$ is the plasma frequency, ϵ_0 is the electric constant, n_e the electron concentration ($n_e^{-1} = 4\pi\bar{r}^3/3$, $\bar{r}$ is the average distance between the conduction electrons), m^* the effective electron mass, ϵ^{∞} the component describing the contribution of the ionic core to the metal dielectric permittivity, and γ the relaxation rate. Note that the relaxation rate in nanostructures can be substantially different from its counterpart for 3D metals. This is a result of the dominance of scattering at nanosystem's boundaries over the contributions made by other scattering channels such as the scattering by phonons, impurities, or structural defects. In this case, formula

(17), instead of γ, will include $\gamma_{\rm eff}^{\perp(\parallel)}$ determined as follows [29]:

$$\gamma_{\rm eff}^{\perp(\parallel)} = \gamma_{\rm bulk} + \gamma_{\rm s}^{\perp(\parallel)} + \gamma_{\rm rad}^{\perp(\parallel)}, \tag{18}$$

where $\gamma_{\rm bulk}$ is the relaxation rate in a 3D metal, and $\gamma_{\rm s}^{\perp(\parallel)}$ are the transverse (longitudinal) relaxation rates associated with the scattering at the surface. In the case of axial and radial motions of electrons in the nanocylinder, $\gamma_{\rm s}^{\perp(\parallel)}$ are determined by the formulas [30] (see Appendix A)

$$\gamma_{\rm s}^{\parallel} = 0, \tag{19}$$

$$\gamma_{\rm s}^{\perp} = \frac{27\pi}{128\,(\epsilon_{\rm m}+1)}\left(\frac{\omega_p}{\omega}\right)^2\frac{v_{\rm F}}{a}. \tag{20}$$

The last summand on the left-hand side of Eq. (18) arises due to the fact that, in addition to the surface attenuation, the radiation one plays an important role in the decay of surface plasmons. It becomes especially appreciable, as the nanocylinder radius increases. The quantities $\gamma_{\rm rad}^{\perp(\parallel)}$ are determined by the relations [29] (see Appendix A)

$$\gamma_{\rm rad}^{\parallel} = 0; \tag{21}$$

$$\gamma_{\rm rad}^{\perp} = \frac{3}{128}\frac{V_{\rm c}}{\sqrt{\epsilon_{\rm m}\,(\epsilon^{\infty}+\epsilon_{\rm m})}}\left(\frac{\omega_p}{c}\right)^3\left(\frac{\omega_p}{\omega}\right)^2\frac{v_{\rm F}}{a}, \tag{22}$$

where $V_{\rm c}$ is the volume of a metal nanocylinder.

The absorption and scattering cross-sections are determined by the expressions [27]

$$C_{\rm abs} = \frac{\omega\sqrt{\epsilon_{\rm m}}}{c}\,{\rm Im}\left(\frac{2}{3}\alpha_{@}^{\perp}+\frac{1}{3}\alpha_{@}^{\parallel}\right), \tag{23}$$

$$C_{\rm sca} = \frac{\omega^4\epsilon_{\rm m}^2}{6\pi c^4}\left(\frac{2}{3}\left|\alpha_{@}^{\perp}\right|^2+\frac{1}{3}\left|\alpha_{@}^{\parallel}\right|^2\right), \tag{24}$$

where c is the speed of light.

2.2. Surface Plasmon Resonance Frequency

From the plasmon resonance condition ${\rm Re}\,\epsilon_{\rm c}^{\perp} = \tilde{\epsilon}_{\rm c}^{(+)}$, it follows that

$${\rm Re}\,\epsilon_{\rm c}^{\perp}\,(\omega_{sp}) = -\epsilon_{\rm ox}\frac{(1+\beta_{\rm c})\,\epsilon_{\rm m}+(1-\beta_{\rm c})\,\epsilon_{\rm ox}}{(1+\beta_{\rm c})\,\epsilon_{\rm ox}+(1-\beta_{\rm c})\,\epsilon_{\rm m}}. \tag{25}$$

Using formula (17), this expression can be represented in the form

$$\epsilon^{\infty}-\frac{\omega_p^2}{\gamma_{\rm eff}^{\perp 2}+\omega_{sp}^2} = -\epsilon_{\rm ox}\frac{(1+\beta_{\rm c})\,\epsilon_{\rm m}+(1-\beta_{\rm c})\,\epsilon_{\rm ox}}{(1+\beta_{\rm c})\,\epsilon_{\rm ox}+(1-\beta_{\rm c})\,\epsilon_{\rm m}}.$$

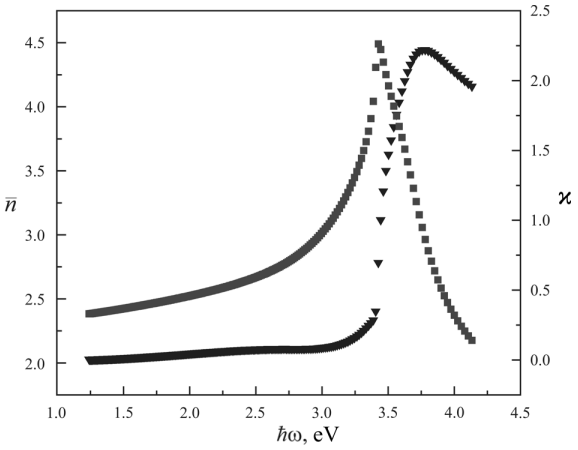

Fig. 2. Experimental frequency dependences of the refractive and extinction indices for Ag_2O [28]

Table 1. **Coefficients of approximating polynomials**

i	$\bar{n}\,(\omega)$		$\varkappa\,(\omega)$	
	c_i	d_i	$\tilde{c}_i$	$\tilde{d}_i$
0	33.731	–197.68	4.8343	-10^6
1	–96.347 c	178.05 c	–15.419 c	$2\cdot 10^6$ c
2	120.63 c^2	–51.055 c^2	20.103 c^2	$-2\cdot 10^6$ c^2
3	–78.889 c^3	4.7611 c^3	–13.771 c^3	530287 c^3
4	28.94 c^4	0	5.237 c^4	–104982 c^4
5	–5.393 c^5	0	–1.0461 c^5	11076 c^5
6	0.419 c^6	0	0.0856 c^6	–486.57 c^6

From whence, for the frequency of surface plasmons, we can write the relation

$$\omega_{sp} = \sqrt{\frac{\omega_p^2}{\epsilon^{\infty}+\epsilon_{\rm ox}\frac{(1+\beta_{\rm c})\epsilon_{\rm m}+(1-\beta_{\rm c})\epsilon_{\rm ox}}{(1+\beta_{\rm c})\epsilon_{\rm ox}+(1-\beta_{\rm c})\epsilon_{\rm m}}}-\gamma_{\rm eff}^{\perp 2}}. \tag{26}$$

Substituting Eqs. (20) and (22) into Eq. (26) and squaring the both parts of the result, we obtain the formula

$$\omega_{sp}^2 = \frac{\omega_p^2}{\epsilon^{\infty}+\epsilon_{\rm ox}\frac{(1+\beta_{\rm c})\epsilon_{\rm m}+(1-\beta_{\rm c})\epsilon_{\rm ox}}{(1+\beta_{\rm c})\epsilon_{\rm ox}+(1-\beta_{\rm c})\epsilon_{\rm m}}} - \left[\gamma_{\rm bulk}+\mathscr{B}\left(\frac{\omega_p}{\omega_{sp}}\right)^2\frac{v_{\rm F}}{a}\right]^2, \tag{27}$$

where the notation

$$\mathscr{B} = \frac{9\pi}{\epsilon_{\rm m}+1}+\frac{V}{\sqrt{\epsilon_{\rm m}\,(\epsilon^{\infty}+\epsilon_{\rm m})}}\left(\frac{\omega_p}{c}\right)^3$$

was introduced. Expression (27) is reduced to the following algebraic equation of the sixth order:

$$\omega_{sp}^6 - \left[\frac{\omega_p^2}{\epsilon^\infty + \epsilon_{\rm ox}\frac{(1+\beta_{\rm c})\epsilon_{\rm m}+(1-\beta_{\rm c})\epsilon_{\rm ox}}{(1+\beta_{\rm c})\epsilon_{\rm ox}+(1-\beta_{\rm c})\epsilon_{\rm m}}} - \gamma_{\rm bulk}^2\right]\omega_{sp}^4 +$$

$$+ 2\gamma_{\rm bulk}\mathscr{B}\omega_p^2\frac{\upsilon_{\rm F}}{a}\omega_{sp}^2 + \mathscr{B}^2\omega_p^4\frac{{\upsilon_{\rm F}}^2}{a^2} = 0. \quad (28)$$

Since the last two summands on the left-hand side of Eq. (28) are small in comparison with the first two, this equation can be solved by the iteration method,

$$\omega_{sp} = \omega_{sp}^{(0)} + \omega_{sp}^{(1)} + ..., \quad (29)$$

where

$$\omega_{sp}^{(0)} = \sqrt{\frac{\omega_p^2}{\epsilon^\infty + \epsilon_{\rm ox}\frac{(1+\beta_{\rm c})\epsilon_{\rm m}+(1-\beta_{\rm c})\epsilon_{\rm ox}}{(1+\beta_{\rm c})\epsilon_{\rm ox}+(1-\beta_{\rm c})\epsilon_{\rm m}}} - \gamma_{\rm bulk}^2}. \quad (30)$$

Substituting expression (29) into Eq. (28), we obtain the formula for the first-order correction,

$$\omega_{sp}^{(1)} = -\frac{\mathscr{B}\omega_p^2\frac{\upsilon_{\rm F}}{a}\left[\mathscr{B}\omega_p^2\frac{\upsilon_{\rm F}}{a} + 2\gamma_{\rm bulk}{\omega_{sp}^{(0)}}^2\right]}{2\omega_{sp}^{(0)}\left[\omega_{sp}^{(0)4} + 2\gamma_{\rm bulk}\mathscr{B}\omega_p^2\frac{\upsilon_{\rm F}}{a}\right]}. \quad (31)$$

Hence, the account for the classical size effects diminishes the frequency of surface plasmons.

Consider the limiting cases of thick and thin oxide layers. The parameter $\omega_{sp}^{(1)}$ is determined by expression (31) in both cases. At the same time, the corresponding formulas for $\omega_{sp}^{(0)}$ are different. For thick oxide layers ($\beta_{\rm c} \to 0$), we have

$$\omega_{sp}^{(0)} = \sqrt{\frac{\omega_p^2}{\epsilon^\infty + \epsilon_{\rm ox}} - \gamma_{\rm bulk}^2}. \quad (32)$$

For thin oxide layers, $\beta_{\rm c} \to 1$, and (see Appendix B) we obtain

$$\omega_{sp}^{(0)} = \sqrt{\frac{\omega_p^2}{\epsilon^\infty + \epsilon_{\rm ox}\frac{(1+\beta_{\rm c})\epsilon_{\rm m}+(1-\beta_{\rm c})\epsilon_{\rm ox}}{(1+\beta_{\rm c})\epsilon_{\rm ox}+(1-\beta_{\rm c})\epsilon_{\rm m}}} - \gamma_{\rm bulk}^2} \cong$$

$$\cong \sqrt{\frac{\omega_p^2}{\epsilon^\infty + \epsilon_{\rm m}} - \gamma_{\rm bulk}^2}\times$$

$$\times\left[1 - (1-\beta_{\rm c})\frac{\omega_p^2\left(\epsilon_{\rm ox}^2 - \epsilon_{\rm m}^2\right)}{4\epsilon_{\rm ox}(\epsilon^\infty + \epsilon_{\rm m})^2\left(\frac{\omega_p^2}{\epsilon^\infty+\epsilon_{\rm m}} - \gamma_{\rm bulk}^2\right)}\right]. \quad (33)$$

The numerical calculations below will be carried out using formulas (2), (23), (24) with regard for Eqs. (3), (4), and (17)–(22).

Table 2. **Metal parameters ($a_0 = \hbar^2/(m_e e^2)$ is the Bohr radius)**

Parameter	Al	Cu	Ag
r_s/a_0 [31]	2.07	2.11	3.02
ϵ^∞	0.7	12.03 [32]	3.7 [32]
m^*/m_e	1.48 [33]	1.49 [34]	0.96 [34]
τ, fs [31]	8	27	40

Table 3. **Dielectric permittivities of oxides, $\epsilon_{\rm ox}$, and matrix, $\epsilon_{\rm m}$**

$\epsilon_{\rm ox}$		$\epsilon_{\rm m}$
Al_2O_3	Cu_2O	Teflon
3.13 [35]	3.7 [36]	2.3 [37]

3. Calculation Results and Their Discussion

The calculations were carried out for two-layer nanocylinders Al@Al_2O_3, Cu@Cu_2O, and Ag@Ag_2O embedded in Teflon. The nanocylinders had various radii and various thicknesses of the oxide layer. The relevant parameters of the metals are presented in Table 2, and the dielectric permittivities of the oxides and Teflon in Table 3.

In Figs. 3 and 4, the frequency dependences of the real and imaginary parts and the absolute values of the transverse and longitudinal, respectively, components of the polarizability of Cu@Cu_2O nanocylinders with various metal-core radii, a, and various thicknesses of the oxide layer, t, are plotted. As one can see, the real part of the transverse polarizability component is an alternating function of the frequency (Fig. 3, *a*), and the absolute value of polarizability is larger for larger radii of the metal core, if the oxide layer thickness is constant (the sequence of curves $2 \to 4 \to 5$), which corresponds to higher metal contents in the wire. Furthermore, a "blue" shift of the Re $\alpha_\perp$ maximum is observed, as the oxide layer thickness decreases. Unlike Re $\alpha_\perp$, the quantity Re $\alpha_\parallel$ is always negative in the examined frequency interval and has the same order of magnitude (Fig. 4, *a*).

The dependence Im $\alpha_\perp(\hbar\omega)$ has a well-pronounced maximum (Fig. 3, *b*), which also undergoes a "blue" shift, as the oxide layer thickness t decreases (the sequence of curves $3 \to 2 \to 1$) or the core radius a

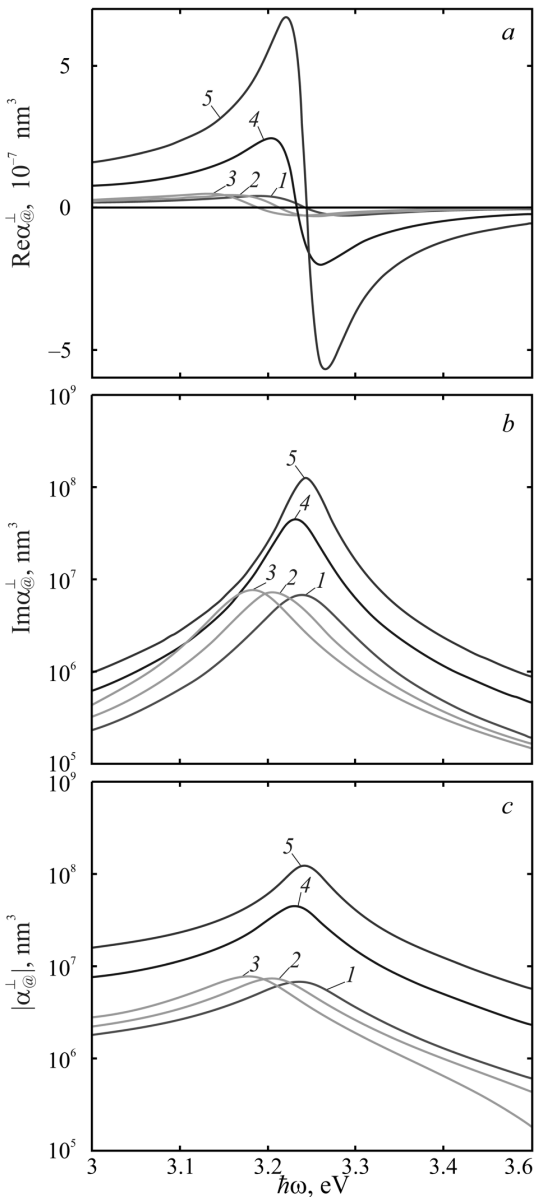

Fig. 3. Frequency dependences of the real (*a*) and imaginary (*b*) parts and the absolute value (*c*) of the transverse polarizability component of Cu@Cu_2O nanocylinders: $a = 10$ nm, $t = 2$ nm (*1*); $a = 10$ nm, $t = 5$ nm (*2*); $a = 10$ nm, $t = 10$ nm (*3*); $a = 20$ nm, $t = 5$ nm (*4*); $a = 30$ nm, $t = 5$ nm (*5*)

increases (the sequence of curves $2 \to 4 \to 5$). The imaginary part of the longitudinal component of the polarization is a decreasing function of the frequency far from the plasmon resonance (Fig. 4, *b*). In the plasmon resonance region, Im $\alpha_{\parallel}$ weakly decreases, as the frequency grows (see the inset in Fig. 4, *b*).

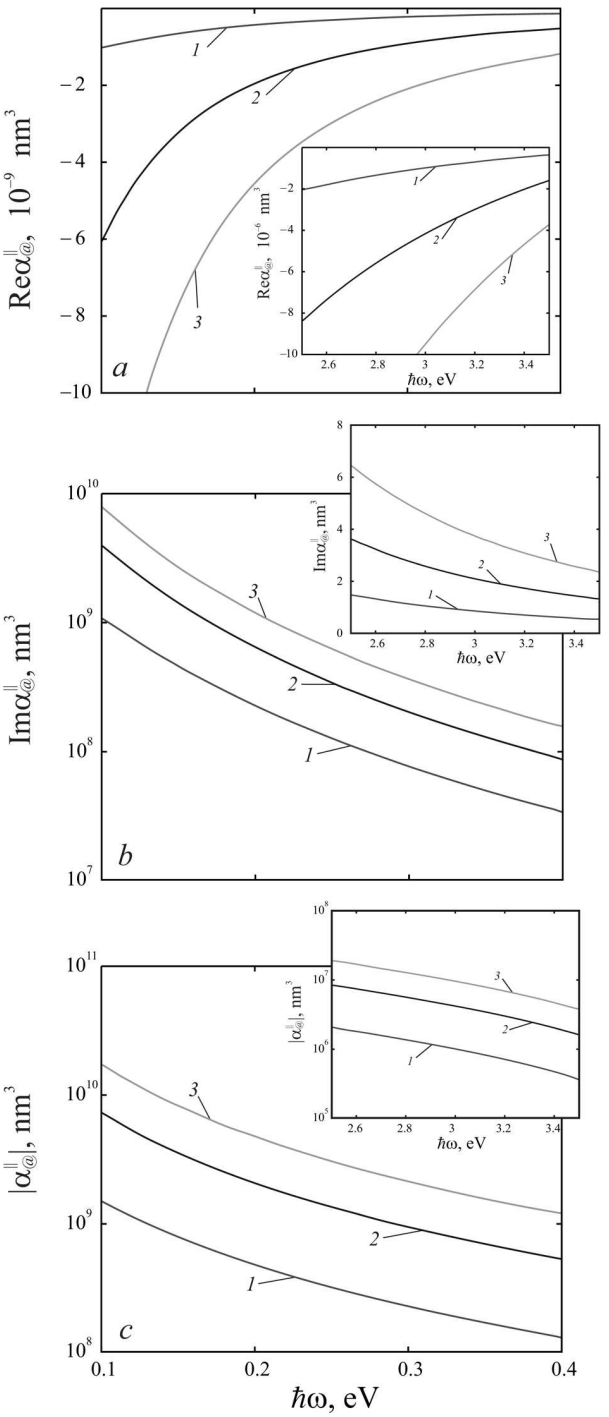

Fig. 4. Frequency dependences of the real (*a*) and imaginary (*b*) parts and the absolute value (*c*) of the longitudinal polarizability component of Cu@Cu_2O nanocylinders: $a = 10$ nm, $t = 2$ nm (*1*); $a = 10$ nm, $t = 5$ nm (*2*); $a = 10$ nm, $t = 10$ nm (*3*)

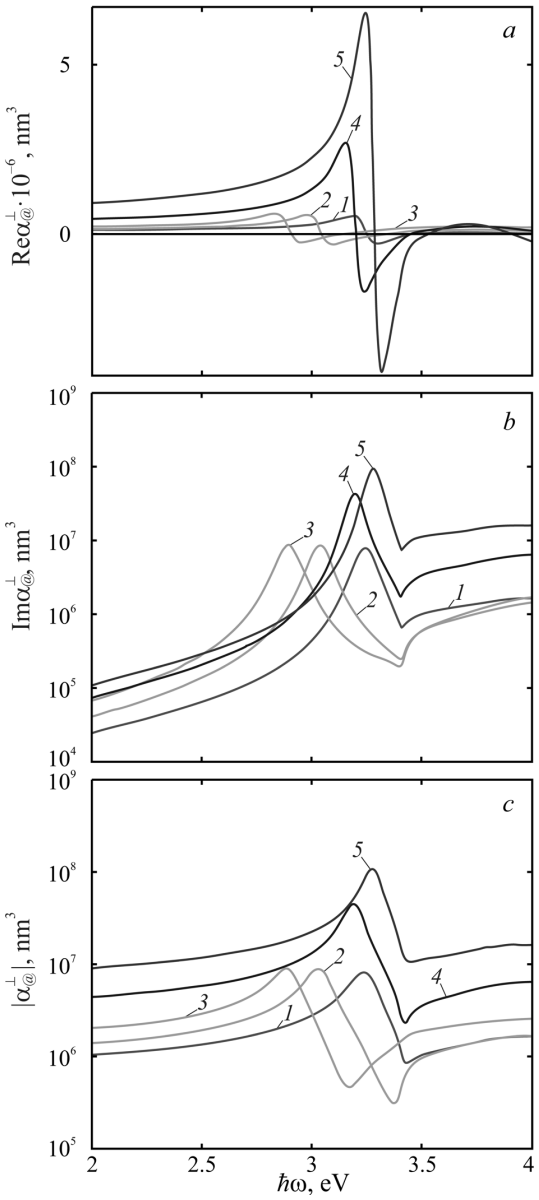

Fig. 5. Frequency dependences of the real (a) and imaginary (b) parts and the absolute value (c) of the transverse polarizability component of Ag@Ag_2O nanocylinders: $a = 10$ nm, $t = 2$ nm (*1*); $a = 10$ nm, $t = 5$ nm (*2*); $a = 10$ nm, $t = 10$ nm (*3*); $a = 20$ nm, $t = 5$ nm (*4*); $a = 30$ nm, $t = 5$ nm (*5*)

The frequency dependences of $|\alpha_\perp|$ and $|\alpha_\parallel|$ are qualitatively similar to the dependences Im $\alpha_\perp(\hbar\omega)$ and Im $\alpha_\parallel(\hbar\omega)$, because the real and imaginary parts become comparable with each other only near the plasmon resonance frequency (Figs. 3, c and 4, c). Analogous calculations for Al@Al_2O_3 nanocylinders

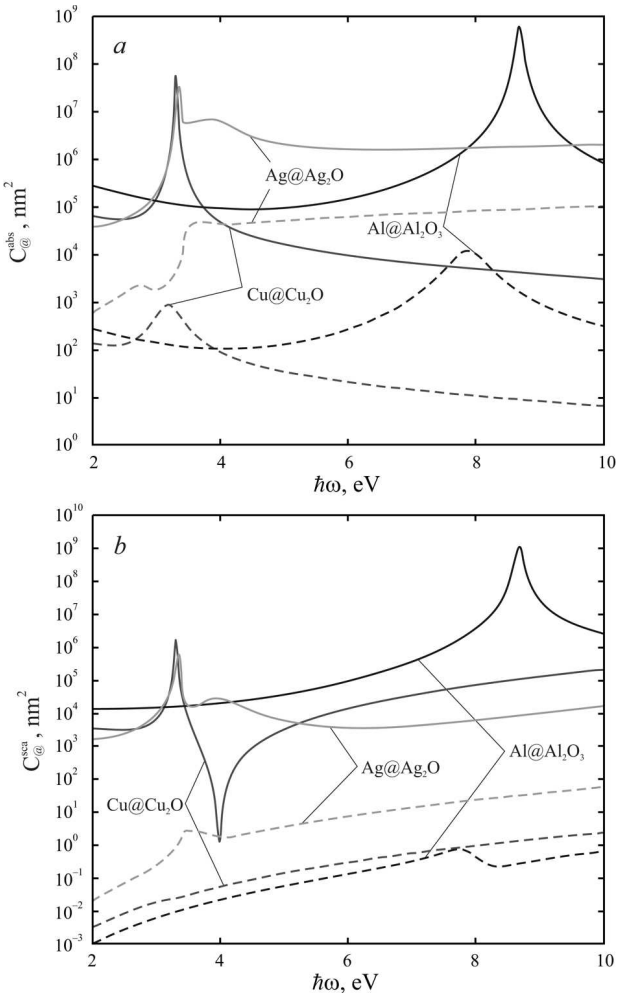

Fig. 6. Frequency dependences of the absorption (a) and scattering (b) cross-sections for layered nanocylinders composed of different metals at $\beta_c = 0.1$ (solid curves) and 0.9 (dashed curves)

also demonstrate a "blue" shift of plasmon resonances, as the oxide layer thickness t decreases or the metal core radius a increases.

The plots of the frequency dependences of Re $\alpha_\perp$, Im $\alpha_\perp$, and $|\alpha_\perp|$ for Ag@Ag_2O nanowires are shown in Fig. 5. In the frequency interval $\hbar\omega \leq 3.3$ eV, the corresponding curves are qualitatively similar to their counterparts for Cu@Cu_2O and Al@Al_2O_3 nanocylinders. However, in contrast to the latter cases, all indicated quantities grow with the frequency at $\hbar\omega > 3.3$ eV. Such a behavior is associated with a drastic increase of $\bar{n}(\omega)$ and $\varkappa(\omega)$ for Ag@Ag_2O in this spectral interval.

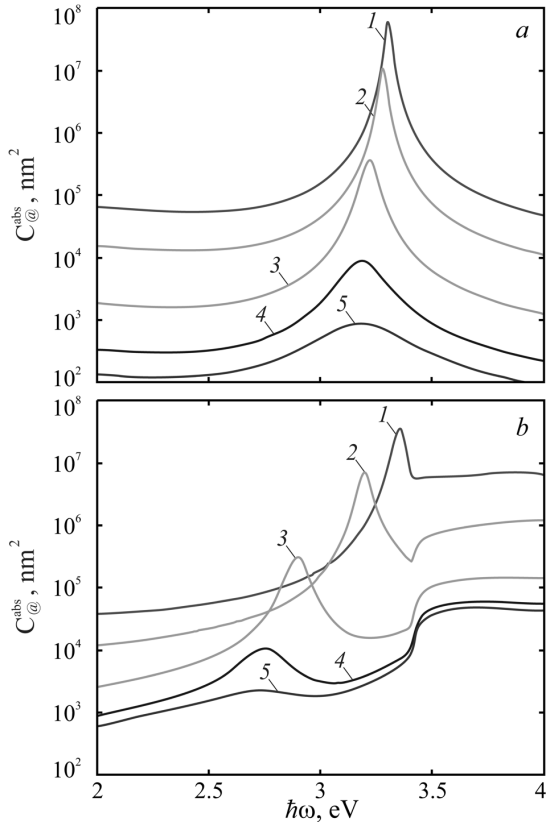

Fig. 7. Frequency dependences of absorption cross-sections for $Cu@Cu_2O$ (*a*) and $Ag@Ag_2O$ (*b*) nanocylinders with a radius of 20 nm and various $\beta_c = 0.1$ (*1*), 0.2 (*2*), 0.5 (*3*), 0.8 (*4*), and 0.9 (*5*)

In Fig. 6, the frequency dependences of the absorption, C_{abs}, and scattering, C_{sca}, cross-sections for the $Ag@Ag_2O$, $Cu@Cu_2O$, and $Al@Al_2O_3$ cylinders are shown for two values of the parameter β_c: 0.1 and 0.9. As one can see, at $\beta_c = 0.1$, the values of C_{abs} and C_{sca} are much larger than in the case $\beta_c = 0.9$ for all composite nanowires and all their compositions considered in this work. At $\beta_c = 0.1$, the quantities C_{abs} and C_{sca} in the cases of $Ag@Ag_2O$ and $Cu@Cu_2O$ cylinders have a maximum at close frequency values, whereas the corresponding maxima for $Al@Al_2O_3$ cylinders are reached at much larger $\hbar\omega$-values, which can be explained by a considerably larger value of ω_p. A comparison between the C_{abs}- and C_{sca}-values at the same $\hbar\omega$'s demonstrates that $C_{\text{abs}} \gg C_{\text{sca}}$. Therefore, the scattering processes can be neglected as compared with the absorption ones.

However, in contrast to the case of $Cu@Cu_2O$ (Fig. 7, *a*) and $Al@Al_2O_3$ nanowires, the absorption cross-section for $Ag@Ag_2O$ nanowires (Fig. 7, *b*) with any thickness of oxide layer increases at the frequencies $\hbar\omega > 3.3$ eV, which is explained by the growth of the refractive and extinction indices.

4. Conclusions

The frequency dependences of the real and imaginary parts and the absolute value of the longitudinal and transverse polarizabilities, as well as the absorption and scattering cross-sections, have been studied for two-layer metal-oxide nanowires. The size dependence of the surface plasmon frequency in those systems is obtained. The limiting cases of "thick" and "thin" oxide layers are considered.

It is found that the reduction of the oxide layer thickness results in the growth of the corresponding absolute values of the real and imaginary parts of the transverse polarizability and in the "blue" shift of the extrema, which is associated with the increase of the metal content in the cylinder. The difference between the "blue" shifts of the real and imaginary parts and the absolute values of the transverse polarization component for the $Cu@Cu_2O$ and $Al@Al_2O_3$ nanocylinders takes place exclusively owing to different values of the bulk concentration of conduction electrons in them.

If the energy of incident radiation exceeds 3.3 eV, the behavior of the frequency dependences of the real and imaginary parts and the absolute value of the transverse polarization component, as well as the scattering and absorption cross-sections, for $Ag@Ag_2O$ nanocylinders substantially differs from that in the case of $Cu@Cu_2O$ and $Al@Al_2O_3$ nanocylinders due to a considerable growth of the refraction and extinction coefficients for Ag_2O in this spectral interval.

It is proved that, owing to the influence of the classical size effects, the frequency of surface plasmons decreases.

APPENDIX A
Calculation of the surface and radiation relaxation rates

The surface and radiation relaxation rates are known to be related to the conductivity via the relations

$$\gamma_{\text{s},\,\beta}\,(\omega) = \frac{\mathcal{L}_\beta \sigma_{\beta\beta}\,(\omega)}{\epsilon_0 g_\beta}, \tag{A.1}$$

$$\gamma_{\mathrm{rad},\,\beta}=\frac{8\pi}{9\sqrt{\epsilon_{\mathrm{m}}}}\left(\frac{\omega_p}{c}\right)^3\frac{R_{\parallel}R_{\perp}^2\,\mathcal{L}_{\beta}\sigma_{\beta\beta}\left(\omega\right)}{\sqrt{\epsilon^{\infty}+\left(\frac{1}{\mathcal{L}_{\beta}}-1\right)\epsilon_{\mathrm{m}}}},\tag{A.2}$$

where $\mathcal{L}_{\beta}$ is the depolarization factor, $g_{\beta}=\epsilon_{\mathrm{m}}+\mathcal{L}_{\beta}\left(1-\epsilon_{\mathrm{m}}\right)$, and $\sigma_{\beta\beta}\left(\omega\right)$ are the diagonal components of the optical conductivity tensor. In the case of an ellipsoid of revolution, the latter can be written in the form

$$\sigma_{\beta\beta}^{\mathrm{el}}\left(\omega\right)=\begin{pmatrix}\sigma_{\perp}\left(\omega\right) & 0 & 0\\ 0 & \sigma_{\perp}\left(\omega\right) & 0\\ 0 & 0 & \sigma_{\parallel}\left(\omega\right)\end{pmatrix}.\tag{A.3}$$

The conductivity of a cylindrical nanowire can be obtained by passing to the limit in the expression for the conductivity of an elongated ellipsoid of revolution with the radii of cross-sections $R_{\perp}$ and $R_{\parallel}$ [30],

$$\sigma_{\perp}(\omega)=\lim_{R_{\parallel}\to\infty}\sigma_{\perp}^{\mathrm{el}}\left(\omega\right),$$

where

$$\sigma_{\perp}^{\mathrm{el}}\left(\omega\right)=\frac{9ne^2}{8m^*}\mathrm{Re}\frac{1}{\nu-i\omega}\int\limits_0^{\frac{\pi}{2}}d\theta\sin^3\theta\,\Psi\left(q\right)|_{\varepsilon=\varepsilon_{\mathrm{F}}},\tag{A.4}$$

$$\Psi\left(q\right)=\frac{4}{3}-\frac{2}{q}+\frac{4}{q^3}-\frac{4}{q^2}\left(1+\frac{1}{q}\right)\mathrm{e}^{-q},$$

$$q=\frac{2R\left(\nu-i\omega\right)}{v'}=q_1-iq_2,$$

$$v'=vR\sqrt{\frac{\sin^2\theta}{R_{\perp}^2}+\frac{\cos^2\theta}{R_{\parallel}^2}},$$

θ is the angle between the electron velocity v and the ellipsoid symmetry axis, and $R=\left(R_{\perp}^2R_{\parallel}\right)^{1/3}$. If the surface scattering dominates, we have $q_1\to 0$ and $q\to -iq_2$, where

$$q_2=\frac{2R_{\perp}}{\nu}\left(1-e_p^2\cos^2\theta\right)^{-1/2}$$

and $e_p^2=\left|1-R_{\perp}^2/R_{\parallel}^2\right|$ is the ellipsoid eccentricity.

Changing the variable $x\equiv 2R_{\perp}\omega\left(1-e_p^2\cos^2\theta\right)^{-1/2}/v$ in integral (A.4) and introducing the notations $\nu_{s,\perp}=v_{\mathrm{F}}/2R_{\perp}$ and $\nu_{s,\parallel}=v_{\mathrm{F}}/2R_{\parallel}$, we obtain

$$\sigma_{\perp}\left(\omega\right)=\frac{9ne^2}{4m^*\omega}\left(\frac{\omega}{\nu_{s,\,\perp}}\right)^2\frac{e_p^2-1}{e_p^3}\int\limits_{\frac{\omega}{\nu_{s,\,\perp}}}^{\frac{\omega}{\nu_{s,\,\parallel}}}\frac{dx}{x^4}\frac{1-\left(\frac{\omega}{\nu_{s,\,\parallel}x}\right)^2}{\sqrt{1-\left(\frac{\omega}{\nu_{s,\,\perp}x}\right)^2}}\times$$

$$\times\left[1-\frac{2}{x}\sin x+\frac{2}{x^2}\left(1-\cos x\right)\right].\tag{A.5}$$

At $R_{\parallel}\to\infty$, we have $e_p\to 1$, $\nu_{s,\,\parallel}\to 0$, $\omega/\nu_{s,\,\parallel}\to\infty$, and

$$\lim_{R_{\parallel}\to\infty}\left(e_p^2-1\right)\left[1-\left(\frac{\omega}{\nu_{s,\parallel}x}\right)^2\right]=$$

$$=-\lim_{R_{\parallel}\to\infty}\frac{R_{\perp}^2}{R_{\parallel}^2}\left(1-\frac{4\omega^2R_{\parallel}^2}{v_{\mathrm{F}}^2x^2}\right)=\frac{4R_{\perp}^2\omega^2}{v_{\mathrm{F}}^2x^2}=\frac{\omega^2}{\nu_s^2x^2},$$

where $\nu_{s,\perp}\equiv\nu_s$. Then,

$$\sigma_{\perp}\left(\omega\right)=\frac{9ne^2}{4m^*\omega}\left(\frac{\omega}{\nu_s}\right)^4\int\limits_{\frac{\omega}{v_s}}^{\infty}\frac{dx}{x^6\sqrt{1-\left(\frac{\omega}{\nu_s x}\right)^2}}\times$$

$$\times\left[1-\frac{2}{x}\sin x+\frac{2}{x^2}\left(1-\cos x\right)\right].\tag{A.6}$$

By changing the variable, $\sin\varphi=\omega/\left(\nu_{s,\,\perp}x\right)$, expression (A.6) can be written in the form

$$\sigma_{\perp}\left(\omega\right)=\frac{9ne^2}{4m^*}\frac{\nu_s}{\omega^2}\int\limits_0^{\frac{\pi}{2}}\sin^4\varphi d\varphi\left[1-2\frac{\nu_s}{\omega}\sin\varphi\sin\frac{\omega}{\nu_s\sin\varphi}+\right.$$

$$\left.+4\left(\frac{\nu_s}{\omega}\right)^2\sin^2\varphi\sin^2\frac{\omega}{2\nu_s\sin\varphi}\right].\tag{A.7}$$

Calculating integral (A.7) and taking into account that $\nu_s\ll\omega$, we obtain

$$\sigma_{\perp}=\frac{9ne^2}{4m^*}\frac{\nu_s}{\omega}\int\limits_0^{\frac{\pi}{2}}\sin^4\varphi d\varphi=\frac{27\pi\epsilon_0}{64}\left(\frac{\omega_p}{\omega}\right)^2\nu_s.\tag{A.8}$$

Substituting this formula into Eq. (A.1) and taking into account that $\mathcal{L}_{\beta}=\mathcal{L}_{\perp}=\frac{1}{2}$, $R_{\perp}=a$, and $R_{\parallel}=l$,, we obtain the following expressions for the surface and radiation relaxation rates:

$$\gamma_s^{\perp}\left(\omega\right)=\frac{27\pi}{128\left(\epsilon_m+1\right)}\left(\frac{\omega_p}{\omega}\right)^2\frac{v_{\mathrm{F}}}{a},\tag{A.9}$$

$$\gamma_{\mathrm{rad}}^{\perp}\left(\omega\right)=\frac{3}{128}\frac{V}{\sqrt{\epsilon_{\mathrm{m}}\left(\epsilon^{\infty}+\epsilon_{\mathrm{m}}\right)}}\left(\frac{\omega_p}{c}\right)^3\left(\frac{\omega_p}{\omega}\right)^2\frac{v_{\mathrm{F}}}{a}.\tag{A.10}$$

Since $\mathcal{L}_{\parallel}=0$, we have

$$\gamma_s^{\parallel}\left(\omega\right)=\gamma_{\mathrm{rad}}^{\parallel}\left(\omega\right)=0.\tag{A.11}$$

APPENDIX B
Calculation of the surface plasmon frequency in a "thin" oxide layer in the zeroth approximation. The case $\epsilon_{\mathrm{ox}}=\mathrm{const}$

In the case of thin oxide layer ($\beta_{\mathrm{c}}\to 1$), we obtain the following formula for the surface plasmon frequency in the zeroth approximation:

$$\omega_{sp}^{(0)}=\sqrt{\frac{\omega_p^2}{\epsilon^{\infty}+\epsilon_{\mathrm{ox}}\frac{(1+\beta_{\mathrm{c}})\epsilon_{\mathrm{m}}+(1-\beta_{\mathrm{c}})\epsilon_{\mathrm{ox}}}{(1+\beta_{\mathrm{c}})\epsilon_{\mathrm{ox}}+(1-\beta_{\mathrm{c}})\epsilon_{\mathrm{m}}}}-\gamma_{\mathrm{bulk}}^2}=$$

$$=\sqrt{\frac{\omega_p^2}{\epsilon^{\infty}+\epsilon_{\mathrm{m}}\frac{1+\frac{1-\beta_{\mathrm{c}}}{1+\beta_{\mathrm{c}}}\frac{\epsilon_{\mathrm{ox}}}{\epsilon_{\mathrm{m}}}}{1+\frac{1-\beta_{\mathrm{c}}}{1+\beta_{\mathrm{c}}}\frac{\epsilon_{\mathrm{m}}}{\epsilon_{\mathrm{ox}}}}}-\gamma_{\mathrm{bulk}}^2}\cong$$

$$\cong\sqrt{\frac{\omega_p^2}{\epsilon^{\infty}+\epsilon_{\mathrm{m}}\left[1+\frac{1-\beta_{\mathrm{c}}}{1+\beta_{\mathrm{c}}}\frac{\epsilon_{\mathrm{ox}}}{\epsilon_{\mathrm{m}}}\right]\left[1-\frac{1-\beta_{\mathrm{c}}}{1+\beta_{\mathrm{c}}}\frac{\epsilon_{\mathrm{m}}}{\epsilon_{\mathrm{ox}}}\right]}-\gamma_{\mathrm{bulk}}^2}\cong$$

$$\cong\sqrt{\frac{\omega_p^2}{\epsilon^{\infty}+\epsilon_{\mathrm{m}}\left[\frac{1-\beta_{\mathrm{c}}}{1+\beta_{\mathrm{c}}}\left(\frac{\epsilon_{\mathrm{ox}}}{\epsilon_{\mathrm{m}}}-\frac{\epsilon_{\mathrm{m}}}{\epsilon_{\mathrm{ox}}}\right)+1\right]}-\gamma_{\mathrm{bulk}}^2}=$$

$$= \sqrt{\frac{\omega_p^2}{\epsilon^\infty + \epsilon_{\rm m} + \frac{\epsilon_{\rm ox}^2 - \epsilon_{\rm m}^2}{\epsilon_{\rm ox}} \frac{1-\beta_{\rm c}}{1+\beta_{\rm c}}} - \gamma_{\rm bulk}^2} =$$

$$= \sqrt{\frac{\omega_p^2}{\epsilon^\infty + \epsilon_{\rm m}} \left[1 + \frac{\epsilon_{\rm ox}^2 - \epsilon_{\rm m}^2}{\epsilon_{\rm ox}\,(\epsilon^\infty + \epsilon_{\rm m})} \frac{1-\beta_{\rm c}}{1+\beta_{\rm c}}\right]^{-1} - \gamma_{\rm bulk}^2} \cong$$

$$\cong \sqrt{\frac{\omega_p^2}{\epsilon^\infty + \epsilon_{\rm m}} \left(1 - \frac{1-\beta_{\rm c}}{1+\beta_{\rm c}} \frac{\epsilon_{\rm ox}^2 - \epsilon_{\rm m}^2}{\epsilon_{\rm ox}\,(\epsilon^\infty + \epsilon_{\rm m})}\right) - \gamma_{\rm bulk}^2} =$$

$$= \sqrt{\frac{\omega_p^2}{\epsilon^\infty + \epsilon_{\rm m}} - \gamma_{\rm bulk}^2} \times$$

$$\times \sqrt{1 - \frac{1-\beta_{\rm c}}{1+\beta_{\rm c}} \frac{\epsilon_{\rm ox}^2 - \epsilon_{\rm m}^2}{\epsilon_{\rm ox}(\epsilon^\infty + \epsilon_{\rm m})^2} \frac{\omega_p^2}{\frac{\omega_p^2}{\epsilon^\infty + \epsilon_{\rm m}} - \gamma_{\rm bulk}^2}} \cong$$

$$\cong \sqrt{\left(\frac{\omega_p^2}{\epsilon^\infty + \epsilon_{\rm m}} - \gamma_{\rm bulk}^2\right)} \times$$

$$\times \left[1 - \frac{1-\beta_{\rm c}}{4} \frac{\epsilon_{\rm ox}^2 - \epsilon_{\rm m}^2}{\epsilon_{\rm ox}(\epsilon^\infty + \epsilon_{\rm m})^2} \frac{\omega_p^2}{\frac{\omega_p^2}{\epsilon^\infty + \epsilon_{\rm m}} - \gamma_{\rm bulk}^2}\right],$$

which coincides with formula (33).

1. K. Ueno, Y. Yokota, S. Juodkazis, V. Mizeikis, H. Misawa. Nano-structured materials in plasmonics and photonics. *Curr. Nanosci.* **4**, 232 (2008).
2. K. Mitamura, T. Imae. Functionalization of gold nanorods toward their applications. *Plasmonics* **4**, 23 (2009).
3. N. Lawrence, L. Dal Negro. Light scattering, field localization and local density of states in coaxial plasmonic nanowires. *Opt. Exp.* **18**, 16120 (2010).
4. J. Zhu, S. Zhao, J.-W. Zhao, J.-J. Li. Dielectric wall controlled resonance light scattering of coated long gold nanowire. *Curr. Nanosci.* **7**, 377 (2011).
5. S.J. Zalyubovskiy, M. Bogdanova, A. Deinega, Y. Lozovik, A.D. Pris, K.H. An, W.P. Hall, R.A. Potyrailo. Theoretical limit of localized surface plasmon resonance sensitivity to local refractive index change and its comparison to conventional surface plasmon resonance sensor. *J. Opt. Soc. Am. A* **29**, 994 (2012).
6. J. Cao, T. Sun, K.T.V. Grattan. Gold nanorod-based localized surface plasmon resonance biosensors: a review. *Sensor. Actuat. B* **195**, 332 (2014).
7. H. Wei, D. Pan, S. Zhang, Z. Li, Q. Li, N. Liu, W. Wang, H. Xu. Plasmon Waveguiding in nanowires. *Chem. Rev.* **118**, 2882 (2018).
8. J. Sun, X. Yu, Z. Li, J. Zhao, P. Zhu, X. Dong, Z. Yu, Z. Zhao, D. Shi, J. Wang, H. Dai. Ultrasonic modification of Ag nanowires and their applications in flexible transparent film heaters and SERS detectors. *Materials* **12** 893 (2019).
9. U. Schoster, A. Dereus. Surface plasmon-polaritons on metal cylinders with dielectric core. *Phys. Rev. B* **64**, 125420 (2001).
10. N.I. Grigorchuk, P.M. Tomchuk. Cross-sections of electric and magnetic light absorption by spherical metallic nanoparticles. The exact kinetic solution. *Ukr. J. Phys.* **51**, 921 (2006).
11. N.I. Grigorchuk. Plasmon resonant light scattering on spheroidal metallic nanoparticle embedded in a dielectric matrix. *Europhys. Lett.* **97**, 45001 (2012).
12. P.M. Tomchuk. Dependence of light scattering cross-section by metal nanoparticles on their shape. *Ukr. Fiz. Zh.* **57**, 553 (2012) (in Ukrainian).
13. A. Murphy, Y. Sonnefraud, A.V. Krasavin, P. Ginzburg, F. Morgan, J. McPhillips, G. Wurtz, S.A. Maier, A.V. Zayats, R. Pollard. Fabrication and optical properties of large-scale arrays of gold nanocavities based on rod-in-a-tube coaxials. *Appl. Phys. Lett.* **102**, 103103 (2013).
14. D.M. Natarov. Modes of a core-shell silver wire plasmonic nanolaser beyond the Drude formula. *J. Optics* **16**, 075002 (2014).
15. A.V. Korotun, A.O. Koval, VV Pogosov. Optical characteristics of bimetallic nanospheres. *Ukr. J. Phys.* **66**, 518. (2021).
16. M.L. Brongersma, V.M. Shalaev. The case for plasmonics. *Science* **328**, 440 (2010).
17. S.A. Maier. *Plasmonics: Fundamentals and Applications* (Springer Science & Business Media, 2007).
18. P. Berini, I. De Leon. Surface plasmon–polariton amplifiers and lasers. *Nat. Photon.* **6**, 16 (2012).
19. P.G. Etchegoin. Plasmonics and spectroscopy. *Phys. Chem. Chem. Phys.* **15**, 5261 (2013).
20. E. Stratakis, E. Kymakis. Nanoparticle-based plasmonic organic photovoltaic devices. *Mater. Today* **16**, 133 (2013).
21. M.L. Dmytruk, S.Z. Malynych. Surface plasmon resonances and their manifestation in the optical properties of nanostructures of precious metals. *Ukr. Fiz. Zh. Ogl.* **9**, 3 (2014) (in Ukrainian).
22. Y.M. Morozov, A.S. Lapchuk, M.L. Fu, A.A. Kryuchyn, H.R. Huang, Z.C. Le. Numerical analysis of end-fire coupling of surface plasmon polaritons in a metal-insulator-metal waveguide using a simple photoplastic connector. *Photon. Res.* **6**, 149 (2018).
23. V.I. Balykin, P.N. Melentyev. Optics and spectroscopy of a single plasmon nanostructure. *Usp. Fiz. Nauk* **188**, 143 (2018) (in Russian).
24. J.M.J. Santillán, L.B. Scaffardi, D.C. Schinca. Quantitative optical extinction-based parametric method for sizing a single core–shell Ag–Ag_2O nanoparticle. *J. Phys. D* **44**, 105104 (2011).
25. J.M.J. Santillán, F.A. Videla, M.B. Fernández van Raap, D.C. Schinca, L.B. Scaffardi. Analysis of the structure, configuration, and sizing of Cu and Cu oxide nanoparticles generated by fs laser ablation of solid target in liquids. *J. Appl. Phys.* **113**, 134305 (2013).
26. A.V. Korotun, A.A. Koval, V.I. Reva. Influence of oxide coating on the electromagnetic radiation absorption by spherical metal nanoparticles. *Zh. Prikl. Spektrosk.* **86**, 549 (2019) (in Russian).

27. M. Liu, P. Guyot-Sionnest. Synthesis and optical characterization of Au/Ag core/shell nanorods. *J. Phys. Chem. B* **108**, 5882 (2004).
28. X.-Y. Gao, H.-L. Feng, J.-M. Ma, Z.-Y. Zhang, J.-X. Lu, Y.-S. Chen, S.-E. Yang, J.-H. Gu. Analysis of the dielectric constants of the Ag_2O film by spectroscopic ellipsometry and single-oscillator model. *Physica B* **405**, 1922 (2010).
29. N.I. Grigorchuk. Radiative damping of surface plasmon resonance in spheroidal metallic nanoparticle embedded in a dielectric medium. *J. Opt. Soc. Am. B* **29**, 3404 (2012).
30. N.I. Grigorchuk, P.M. Tomchuk. Optical and transport properties of spheroidal metal nanoparticles with account for the surface effect. *Phys. Rev. B* **84**, 085448 (2011).
31. N.W. Ashcroft, N.D. Mermin. *Solid State Physics* (Saunders College Publishing, 1976).
32. I.I. Shaganov, T.S. Perova, K. Berwick. The effect of the local field and dipole-dipole interactions on the absorption spectra of noble metals and the plasmon resonance of their nanoparticles. *Photon. Nanostruct. Fund. Appl.* **27**, 24 (2017).
33. W.A. Harrison. *Solid State Theory* (McGraw-Hill, 1970).
34. P.B. Johnson, R.W. Christy. Optical constants of the noble metals. *Phys. Rev. B* **6**, 4370 (1972).
35. J. Zhu, J.-J. Li, J.-W. Zhao. A computational study of the double-bands plasmonic light scattering of Al_2O_3 coated Al nanoshells in the deep-ultraviolet range. *Appl. Surf. Sci.* **314**, 145 (2014).
36. W.Y. Ching, Y.-N. Xu. Ground-state and optical properties of Cu_2O and CuO crystals. *Phys. Rev. B* **40**, 7684 (1989).
37. E.M. Voronkova, B.N. Grechushnikov, G.I. Distler, I.P. Petrov. *Optical Materials for Infrared Technology* (Nauka, 1965) (in Russian).

Received 04.01.21.
Translated from Ukrainian by O.I. Voitenko

А.В. Коротун, Я.В. Карандась, В.І. Рева, І.М. Тітов

ПОЛЯРИЗОВНІСТЬ ДВОШАРОВОГО МЕТАЛ-ОКСИДНОГО НАНОДРОТУ

В роботі одержано співвідношення для частотних залежностей дійсної й уявної частин та модуля компонентів тензора поляризовності, а також перерізів поглинання і розсіювання метал-оксидних нанодротів. Досліджено граничні випадки "товстого" і "тонкого" зовнішнього шару оксиду. Чисельні розрахунки проведено для дротів Al, Cu і Ag, вкритих шаром власного оксиду. Розглянуто випадки, коли діелектрична проникність оксиду є постійною величиною або є функцією частоти. В останньому випадку для визначення цієї залежності було використано апроксимацію експериментальних кривих частотних залежностей показників заломлення та екстинкції. Проаналізовано вплив зміни товщини оксидного шару на поведінку частотних залежностей поляризовності і перерізів поглинання і розсіювання. Встановлено, що наявність оксиду приводить до зменшення частоти поверхневих плазмонів у двошарових нанодротах внаслідок впливу класичних розмірних ефектів.

Ключові слова: метал-оксидний нанодріт, тензор поляризовності, переріз поглинання, переріз розсіювання, поверхневий плазмон, діелектрична функція, розмірна залежність.